ARTICLE

Using autonomous video to estimate the bottom-contact area of longline trap gear and presence–absence of sensitive benthic habitat[1]

Beau Doherty, Samuel D.N. Johnson, and Sean P. Cox

Abstract: Bottom longline hook and trap fishing gear can potentially damage sensitive benthic areas (SBAs) in the ocean; however, the large-scale risks to these habitats are poorly understood because of the difficulties in mapping SBAs and in measuring the bottom-contact area of longline gear. In this paper, we describe a collaborative academic–industry–government approach to obtaining direct presence–absence data for SBAs and to measuring gear interactions with seafloor habitats via a novel deepwater trap camera and motion-sensing systems on commercial longline traps for sablefish (*Anoplopoma fimbria*) within SGaan Kinghlas – Bowie Seamount Marine Protected Area. We obtained direct presence–absence observations of cold-water corals (Alcyonacea, Antipatharia, Pennatulacea, Stylasteridae) and sponges (Hexactinellida, Demospongiae) at 92 locations over three commercial fishing trips. Video, accelerometer, and depth sensor data were used to estimate a mean bottom footprint of 53 m² for a standard sablefish trap, which translates to 3200 m² (95% CI = 2400–3900 m²) for a 60-trap commercial sablefish longline set. Our successful collaboration demonstrates how research partnerships with commercial fisheries have potential for massive improvements in the quantity and quality of data needed for conducting SBA risk assessments over large spatial and temporal scales.

Résumé : Les engins de pêche à la palangre à l'hameçon et au filet-piège pourraient causer des dommages aux zones benthiques sensibles (ZBS) dans l'océan; les risques à grande échelle pour ces habitats demeurent toutefois mal compris en raison des difficultés que présentent la cartographie des ZBS et la mesure de la superficie de contact de ces engins avec le fond. Nous décrivons une approche de collaboration université–industrie–gouvernement visant à obtenir des données directes sur la présence ou l'absence pour des ZBS et à mesurer les interactions des engins avec les habitats du fond marin par l'entremise d'une caméra novatrice pour eau profonde et de systèmes de détection du mouvement montés sur des filets-pièges pour la morue charbonnière (*Anoplopoma fimbria*) dans la zone de protection marine SGaan Kinghlas – mont sous-marin Bowie. Nous avons obtenu des observations directes sur la présence ou l'absence de coraux d'eau froide (alcyonacés, antipathaires, pennatulacés, stylasteridés) et d'éponges (hexactinellides, démosponges) en 92 emplacements lors de trois sorties de pêche commerciale. Des données vidéo, d'accéléromètre et de détecteur de profondeur ont été utilisées pour estimer une empreinte moyenne sur le fond marin de 53 m² pour un filet-piège à morue charbonnière normal, ce qui se traduit par 3200 m² (IC de 95 % = 2400–3900 m²) pour une calée de palangre commerciale de 60 filets-pièges. Cette collaboration fructueuse démontre que les partenariats de recherche avec les pêcheurs commerciaux ont le potentiel de produire d'importantes améliorations de la quantité et de la qualité des données nécessaires à la réalisation d'évaluations des risques pour les ZBS à de grandes échelles spatiales et temporelles. [Traduit par la Rédaction]

Introduction

Sensitive benthic areas (SBAs), such as cold-water coral and sponge communities, occur throughout the world's oceans often providing three-dimensional habitat for fish and invertebrate populations (Krieger and Wing 2002; Buhl-Mortensen et al. 2010; Stone et al. 2015). SBAs and associated communities are prone to damage when contacted by fishing gear, and recovery from such damage can take decades (Sainsbury et al. 1997; Williams et al. 2010; Rooper et al. 2011). Spatial management strategies such as marine protected areas (MPAs) that permanently close large areas to bottom-contact fisheries are increasingly used to limit or avoid damage to SBAs in many parts of the world (Hourigan 2009; Wright et al. 2015). However, for most remote parts of the deep ocean, there is little

information about the locations, diversity, abundance, and composition of SBAs, as well as the potential risks to these habitats from bottom-contact fishing methods other than trawling. Without better information, misplaced MPAs (i.e., both location and size) could have a dual effect of (i) shifting fishing effort to more valuable, yet unprotected, SBA locations and (ii) creating unnecessary fishery economic losses or increases in fishing cost (Lagasse et al. 2015). These potential consequences create strong incentives for the fishing industry to engage in new scientific research aimed at mapping SBA distributions (e.g., Woodby et al. 2009; Rooper et al. 2014; Lagasse et al. 2015), as well as forecasting potential fishery impacts to these habitats (e.g., Welsford et al. 2014b; Eigaard et al. 2016). Such research could better inform ecosystem-based fisheries management that minimizes risks to bottom

B. Doherty, S.D.N. Johnson, and S.P. Cox. Quantitative Fisheries Research Group, School of Resource and Environmental Management, Simon Fraser University, Burnaby, BC V5A 1S6, Canada.

Corresponding author: Sean P. Cox (email: spcox@sfu.ca).

habitats while allowing fisheries to maintain access to fishing grounds where risks of damage are low.

It is reasonably well established that bottom trawling and dredging damage benthic communities by removing large amounts of sessile epifauna and dramatically altering certain benthic communities (Collie et al. 2000; Kaiser et al. 2006; Clark et al. 2016). We know much less about the potential impacts of bottom longline fisheries, even though these fisheries are more common and occur over a wider range of bottom habitats (Heifetz et al. 2009). In general, bottom longline gear (e.g., hook-and-line) is thought to be less damaging because of a much smaller bottom-contact area, lighter weight, and relative stationarity on the seafloor (Hourigan et al. 2007; Pham et al. 2014); however, there is little scientific research available to test this assertion. Bottom longline gear using baited hooks or traps have potential to damage corals and sponges by landing on them when deployed or by dragging over them during retrieval (Eno et al. 2001; Stone 2006; Stone et al. 2015). Lateral movement of the mainline during dragging can create shearing forces that may break corals off at their base, while hooks, lines, and traps can entangle or crush freestanding corals during retrieval (Troffe et al. 2005; Durán Muñoz et al. 2011; Sampaio et al. 2012; Bo et al. 2014; Ewing and Kilpatrick 2014). On the other hand, the extent of dragging that occurs is likely influenced by particular circumstances of, for example, bottom bathymetry, hauling direction, wind, and currents (Eno et al. 2001; Stone 2006). Mainlines for some types of trap gear are also buoyant and may not even contact the bottom. Therefore, unlike trawls and dredges, the footprints from bottom longline gear involve more than a computation of length × width of a tow.

Scientific partnerships among academia, government, and the fishing industry have been used to assess bottom longline impacts on SBAs (Kilpatrick et al. 2011; Durán Muñoz et al. 2011; Sampaio et al. 2012). In this paper, we demonstrate a collaborative, technological approach to improving the scientific information for assessing risks to cold-water corals and sponges from bottom longline trap fisheries. Through an academic–industry–government project, we developed and deployed a novel deepwater trap camera and motion-sensing system on commercial bottom longline trap fishing gear to collect direct observations of potential bottom impacts and benthic community composition.

Understanding the risks to SBAs from bottom longline fisheries requires four general types of information: (1) presence or presence–absence data for mapping suitable habitat for SBAs defined by presence of corals and sponges; (2) the effective bottom-contact area or footprint of gear deployed within the fishing area; (3) the damage or mortality rate arising from gear contact with sensitive habitats or individual organisms; and (4) the recovery rates from damage (Rooper et al. 2011). Mapping habitat suitability for deepwater corals and sponges is challenging because direct observations are typically expensive and difficult to collect over large spatial scales and in remote areas of the deep ocean. By designing our cameras to work on commercial fishing gear, we are able to (i) vastly improve the input data to habitat suitability models for corals and sponges by using direct presence–absence data rather than the typical presence-only data (Hastie and Fithian 2013; Lagasse et al. 2015) and (ii) provide a cost-efficient means of covering the large spatial scales needed to produce high-quality habitat suitability maps. Additionally, depth and accelerometer sensors on our camera systems allowed us to develop a simple algorithm for quantitatively estimating longline trap fishing footprints based on gear behaviour during set, soak, and hauling periods.

Role of industry–academic–government collaboration in deep-sea research

Between 2012 and 2015, bottom-contact fisheries off British Columbia, Canada, generated a mean total landed value of CAD$122 million, with longline hook and longline trap fisheries for Pacific halibut (*Hippoglossus stenolepis*) and sablefish (*Anoplopoma fimbria*) account-

ing for CAD$66 million. Longline fisheries operate along most of the continental slope and shelf (Fig. 1), including within complex terrain (e.g., boulder outcrops, rocky reefs) that is inaccessible by bottom trawl (Sinclair et al. 2005; Wallace et al. 2015). This ability to fish a variety of terrain over a broad area increases the likelihood of bottom contact in areas where cold-water corals and sponges probably occur (Mortensen and Buhl-Mortensen 2004; Woodby et al. 2009).

In 2010, conservation groups in British Columbia questioned the Marine Stewardship Council's certification of British Columbia's sablefish fishery on grounds that there was no information about impacts of bottom longline fishing effort on vulnerable habitats (Furness et al. 2010). In response, Wild Canadian Sablefish, Ltd. (WCS) joined with Simon Fraser University (S.P. Cox) and Fisheries and Oceans Canada (DFO Pacific Region) to design, build, and deploy an autonomous video camera and motion-sensing system capable of operating at extreme depths of 200–1800 m where sablefish occur (Wyeth et al. 2007). The camera system, along with accelerometers and depth sensors, have been deployed annually on selected commercial fishing trips and on the annual stratified-random, fishery-independent sablefish survey that is jointly funded by WCS and DFO (Wyeth et al. 2007).

In this paper, we report the first results from this collaborative academic–industry–government approach to improving the scientific information for protecting cold-water corals and sponges from bottom-contact fishing at SGaan Kinghlas – Bowie (SK-B) Seamount, which is part of the Bowie Seamount MPA created in 2008 under Canada's Oceans Act. The sablefish fishery by longline trap is the only fishing permitted within the SK-B MPA and is restricted to Zone 2 at depths deeper than 457 m (DFO 2015; Fig. 1). Although Zone 2 is greater than 2500 km² in area, the sablefish fishery primarily operates at depths between 457 and 1500 m, resulting in a potential fished area of approximately 200 km². The scientific challenges of finding and protecting sensitive benthic areas at SK-B are indicative of challenges that are occurring, or are likely to occur in the future, in other areas as Canada aims to implement a large-scale MPA strategy (DFO 2005; Government of Canada 2014).
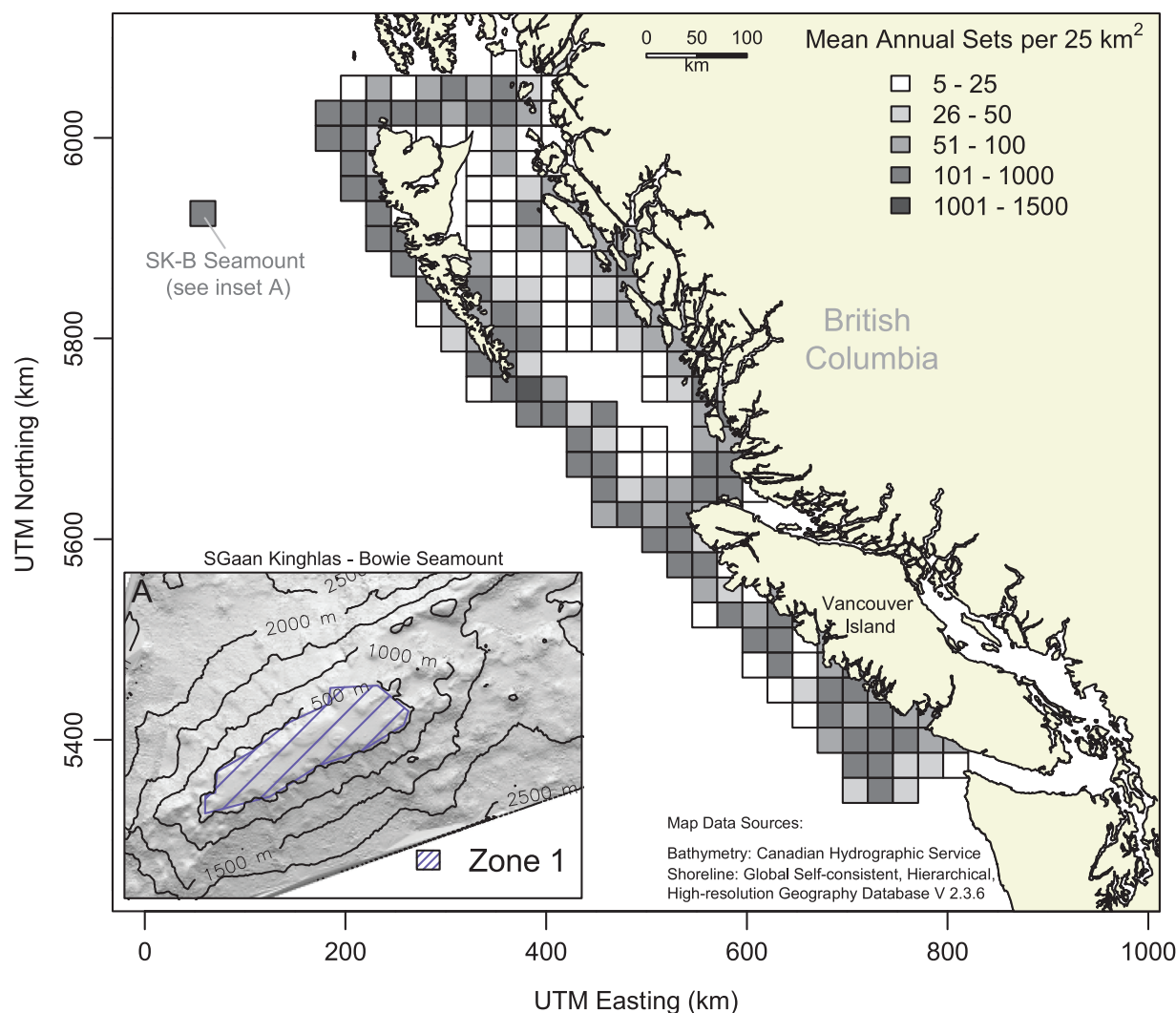
Materials and methods

In this section we first describe (i) the camera system as developed for sablefish trap gear, the sampling protocols, and collection of presence–absence data for deep-sea corals and sponges that is needed for habitat suitability modelling. We then describe (ii) a new Bayesian method for estimating the bottom locations of the trap cameras and, finally, (iii) an algorithm for estimating the bottom-contact area of bottom longline trap gear.

Autonomous video camera system and sampling protocol

The video component of the trap camera system uses a GoPro HD Hero that produces 1080p video and four LED lights (Cree XLamp XM-L) that can generate up to 500 total lumens. The camera, lights, lithium-ion battery pack (Ultra Life UBBL24-FL), depth sensor, and tri-axial accelerometer are all contained within a 3.6 kg stainless steel housing rated to 1500 m depth. A custom circuit board and controller contained inside the housing allows programming the cameras to record video at both regularly timed intervals and using motion-activation thresholds via link to an accelerometer that moderates power delivery to the GoPro camera. The battery pack allows camera deployments up to 48 h with 1 min video recordings every hour.

Over the 2013–2015 period, we deployed the camera systems on commercial fishing traps for sablefish at SK-B (Fig. 2) along with external accelerometers (Actilife wGT3x-BT monitors) and depth–temperature sensors (Sea-Bird SBE 39; Table 1). A total of six trap camera systems were deployed individually in single traps as part of commercial bottom longline sets that each contained between 41 and 60 traps. The vessel position was recorded at the terminal ends of the set, with a linear distance between set endpoints rang-

Fig. 1. Mean annual effort density of bottom longline hook and trap sets (2006–2011) for British Columbia coastal groundfish fisheries and the SGaan Kinghlas – Bowie Seamount (SK-B) Marine Protected Area. The SK-B Zone 1 area (top 457 m contour) is closed to all fishing. [Colour online.]

ing from 1.8 to 4.0 km (median of 3.0 km). Cameras were programmed to record 1 min video clips at 2 h intervals while the trap was stationary on the bottom. Accelerometers within the camera housing system itself were used to trigger additional video recordings of trap movement during gear retrieval at impact forces greater than 0.6*g*. Depth–temperature sensors recorded at 10 s intervals. Traps are a conical design with a circular steel base (hoop) of 137 cm diameter extending to a smaller circular top 84 cm in diameter (Fig. 2). During fishing, the traps are connected to stainless steel rings on a polypropylene groundline with approximately 60 kg chain anchors at each end to reduce groundline movement (Wyeth et al. 2007). Fishing sets at SK-B are normally deployed along the slopes of the seamount perpendicular to contour lines with one end of the set in shallow water and the other in deeper water. Gear retrieval typically begins at the deep end of the set, and attempts are made to minimize dragging by pulling the string of connected traps straight up off the bottom.

Video clips were reviewed to record observations of all species, benthic habitat, physical substrate, and gear substrate interactions (Fig. 3). All epifauna were identified to the lowest taxonomic rank possible, which was typically the order or family level. Lower taxonomic identification of deepwater corals and sponges to genus or species was limited by (*i*) a lack of close-up images required to identify distinguishing morphology; (*ii*) views of specimens

obstructed by traps, netting, boulders, or other animals; (*iii*) an absence of physical samples that are often needed to confirm identification to species level; and (*iv*) the potential for observations of previously undescribed species (Cairns 2007; Austin et al. 2013; Reiswig 2015). Additional video still frames of coral and sponge observations and a list of the resources used for taxa identification are available in Doherty and Cox (2017).

Estimating trap landing locations

We used a Bayesian approach to estimate the bottom landing coordinates of sablefish traps from 99 fishing sets at SK-B that were deployed with depth sensors. Discrete posterior probability distributions were produced on a square grid by combining trap surface-deployment coordinates, multibeam bathymetry, and depth sensor data recorded during each set's soak time. We give symbols and notation for the location estimator in Table 2, with the full statistical model given in Table 3.

For each set *i* we recorded the total number of traps deployed, $N^{(i)}$, and the relative position $n^{(i)}$ of the camera trap (and depth sensor) along the deployment track $(x_{START}^{(i)}, y_{START}^{(i)})$. We estimated the surface deployment coordinates $\mu^{(i)} = (\tilde{x}^{(i)}, \tilde{y}^{(i)})$ of the camera trap by taking a weighted mean of the deployment track start and end locations (Table 3, eqs. 3.1–3.3). We assigned the median Sea-Bird depth

Fig. 2. Close-up configuration of the camera housing, external accelerometer, and depth–temperature sensor in a commercial sablefish trap (top left). The trap's front mesh panel has been cut out to provide unobstructed field of view (top right). The bottom diagram displays the different components of the fishing gear and configuration for a 3 km long bottom longline sablefish trap set with 59 traps (traps 2–28 and 32–58 not shown). [Colour online.]
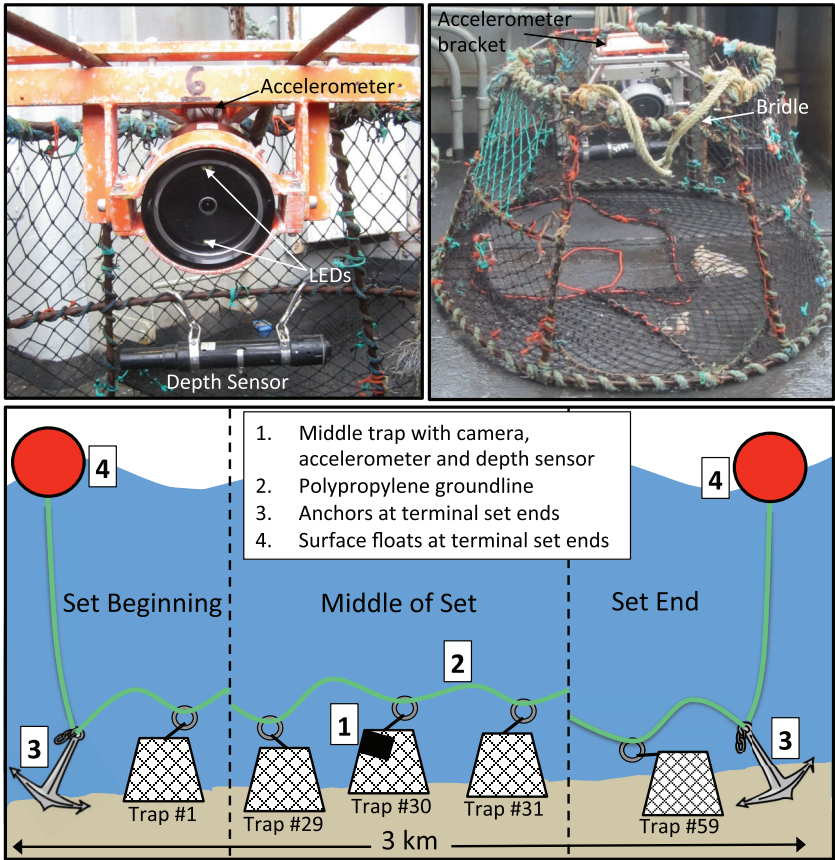

Table 1. Summary of data collection requirements and the number of commercial sets at SGaan Kinghlas–Bowie Seamount (SK-B) (e.g. sample sizes) included in the three different analyses.

Estimates–observations	Sets	Year(s)	Equipment
Coral and sponge presence–absence	92	2013–2015	Camera
Trap location	99	2013–2015	Depth sensor
Trap movement	20	2015	Depth sensor, accelerometer, cameras

measurement during the period that the trap was stationary on the seafloor as the observed landing depth $\hat{d}^{(i)}$.

For each set i we produced a 10 m by 10 m resolution Bayesian poster grid $P_{j,k}^{(i)}$ from a depth likelihood grid $L_{j,k}^{(i)}$ and spatial prior grid $p_{j,k}^{(i)}$ (Table 3, eqs. 3.4–3.8). The depth likelihood grid $L_{j,k}^{(i)}$ is computed using a normal density function with mean $\hat{d}^{(i)}$ and variance τ^2. The depth likelihood function (Table 3, eq. 3.6) assumes that for each 10 m by 10 m cell (j, k), deviations between the bathymetry $b_{j,k}^{(i)}$ for that cell and the observed depth $\hat{d}^{(i)}$ are normally distributed. We obtained bathymetry values for the depth likelihood grid from 10 m resolution multibeam bathymetry data for SK-B (Canadian Hydrographic Services; Halcro 2000). We set the variance of the observation error distribution as $\tau^2 = 1$ m^2, based on our assumption that 99% of the true trap depths lie within 3 m of the observed depth reading $\hat{d}^{(i)}$. This assumption reflects our knowledge about the instrument's precision and the position of the accelerometer within the trap, as well as uncer-

tainty about trap orientations, tidal changes, and wave actions affecting the precision of the depth readings.
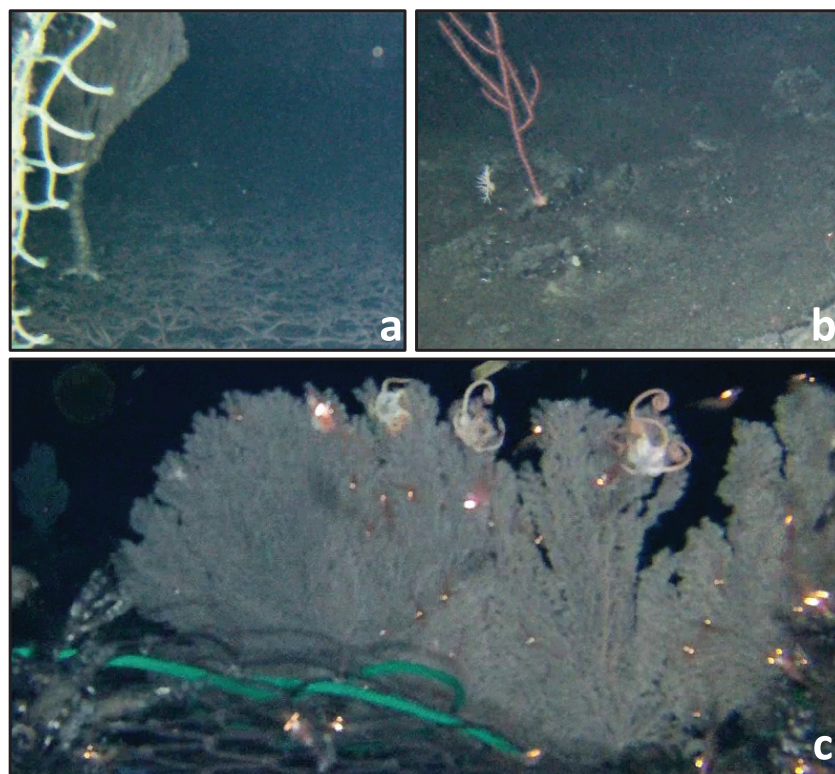
The spatial prior grid is computed from a bivariate normal density with mean $\mu^{(i)}$ (i.e., the initial deployment location) and covariance matrix Σ. We used the spatial prior distribution (Table 3, eq. 3.7) to penalise the distance of each grid cell's centre $\Theta_{j,k}^{(i)}$ from the estimated deployment location $\mu^{(i)}$. Deviations from the estimated deployment location are assumed to have a diagonal covariance matrix Σ with $\Sigma_{1,1} = \Sigma_{2,2} = (\bar{l}/6)^2$, where $\bar{l}$ is the mean length of a deployment track, calculated as the linear distance between deployment locations of anchors at the start and end of each set. We chose this covariance matrix based on the assumption that 99% of the bottom landing locations of the trap would occur within a circle centred at the deployment location with diameter equal to the length of an average set.

We performed all calculations for the Bayesian posterior grids using the raster package in the R statistical language (R Core Team 2015). The raster package enables grids to be manipulated arithmetically, allowing for bathymetry and spatial grids to be directly substituted for the variables in likelihood and prior functions (Table 3, eqs. 3.6, 3.7) to produce likelihood and prior grids, as well as allowing for grids to be combined.

We quantified trap displacement from the deployment location using three metrics from the Bayesian posterior grid. First, we calculated the posterior mean distance of a trap from deployment location as

$$\hat{\mu}^{(i)} = \sum_{(j,k)} P_{j,k}^{(i)} \cdot (100j^2 + 100k^2)^{1/2}$$

Fig. 3. Video still images collected from trap cameras during commercial fishing of (*a*) bamboo coral (Family Isididae) and substrate with dense coverage of brittle stars, (*b*) *Swiftia simplex* (larger specimen) and small white hydrocoral (Family Stylasteridae), and (*c*) *Parastenella* sp. serving as habitat for shrimp and basket stars. Trap mesh is visible in panels (*a*) and (*c*). [Colour online.]

Second, we computed the distance from the deployment location to the posterior mode, analogous to a maximum posterior density estimate. Finally, we estimated the distance to the posterior medoid, defined as the posterior grid cell with density greater than 0.0001 that was closest to the ordered pair of medians of the marginal easting and northing distributions.

Owing to the large number of grid cells (62 500), a uniform probability distribution would assign a probability of 0.0016% to the event that the camera trap lands in any single 10 m × 10 m square grid cell; therefore, we calculated uncertainty in displacement of traps from deployment locations for each Bayesian posterior grid as the minimum required size of a square subgrid centred at a given location and capturing 50% or 95% of the posterior distribution. We used the posterior mode and medoid as centres for the observations because the expected and median values often occur in areas of vanishingly small density.

Trap movement and bottom-contact estimates

We used depth measurements, accelerometer data, and video recordings to classify different periods of trap movement and to estimate the bottom-contact area of traps during gear retrieval for 2015 commercial fishing sets. Observations from 2013–2014 sets, as wells as three sets from 2015, were excluded from analyses because time stamps from video recordings and motion-sensing equipment could not be reliably synchronized. We analysed 21 different commercial fishing sets from 2015 and focussed our analysis on the last hour of fishing when gear retrieval occurs, because video observations showed that traps were stationary prior to the last hour. The last hour of the set was determined as the final 60 min for which depth sensor readings were deeper than 5 m.

We developed an algorithm for classifying gear behaviour during 1 s intervals over the last hour (i.e., 3600 s) of each set using the following measurements:

- depth sensor measurements (d_t),
- the depth change over 10 s intervals ($d_t - d_{t-10}$),
- acceleration (a_t),
- acceleration variance over 10 s intervals ($\sigma^2_{t:(t+10)}$),
- and observed trap movement from 1 min video.

Trap movement was classified as either "stationary", "dragging", or "suspended" (Figs. 4, 5), using the following algorithm:

Step 1. Define start and end times for drag window:

(*a*) Choose the start of the drag window as the first time step subject to (s.t.) any one of three conditions being true, i.e.:

$$t^{\text{start}} = \min\left\{ t \text{ s.t. } \begin{array}{l} |d_t - d_{t-10}| > 5 \text{ cm; or} \\ \log\sigma^2_{t:(t+10)} < -10 \text{ g}^2\text{; or} \\ a_t > a_{\text{video}} \end{array} \right\}$$

where a_{video} is the camera's acceleration trigger threshold for recording videos during gear movement.

(*b*) Choose the end of the drag window as the first time step subject to two conditions being simultaneously true:

$$t^{\text{end}} = \min\left\{ t \text{ s.t. } t > t^{\text{start}} \text{ and } (d_t - d_{t-10}) > 6 \text{ cm} \right\}$$

Step 2. Determine the class $C_{(t-10):t}$ of trap behaviour over 10 s intervals for each t within the drag window:

$$C_{(t-10):t} = \begin{cases} \text{"stationary"} & d_t = d_{t-10} \\ \text{"dragging"} & d_t \neq d_{t-10} \end{cases}$$

Step 3. Set the classes of trap behaviour to $C_{1:(t^{\text{start}}-1)} =$ "stationary" for each t prior to the drag window and $C_{(t^{\text{end}}+1):3600} =$ "suspended" for each t after the drag window.

Table 2. Symbol definitions for the trap location estimator and the trap movement classifier.

Symbol	Definition
Trap location estimator	
x	Eastings coordinate
y	Northings coordinate
$\Theta_{j,k}^{(i)}$	Trap location estimator grid cell centres for trap string i
$b_{j,k}^{(i)}$	Bathymetry data (m) from cell (j, k) of grid for trap string i
$\hat{d}^{(i)}$	Median depth measurement (m) of trap string i while trap classified as stationary
$x_{START}^{(i)}$	Eastings coordinate of start of deployment track for trap string i
$y_{START}^{(i)}$	Northings coordinate of start of deployment track for trap string i
$x_{END}^{(i)}$	Eastings coordinate of end of deployment track for trap string i
$y_{END}^{(i)}$	Northings coordinate of end of deployment track for trap string i
$N^{(i)}$	Total number of traps deployed in set i
$n^{(i)}$	Ordinal number indicating position in set of trap containing Sea-Bird depth sensor
$\tilde{x}^{(i)}$	Estimated eastings coordinate of Sea-Bird deployment location
$\tilde{y}^{(i)}$	Estimated northings coordinate of Sea-Bird deployment location
τ^2	Depth measurement error variance
Σ	Covariance matrix for spatial prior distribution
$\bar{l}$	Mean length of a trap deployment track
$L_{j,k}^{(i)}$	Likelihood function value at grid cell reference (j, k) for set i
$p_{j,k}^{(i)}$	Prior probability at grid cell reference (j, k) for set i
$P_{j,k}^{(i)}$	Posterior probability at grid cell reference (j, k) for set i
Trap movement classifier	
d_t	Depth sensor measurements at 10 s intervals
a_t	Acceleration (g) at 1 s intervals
a_{video}	Camera acceleration trigger threshold for motion-activated video recording
$\sigma_{t:(t+10)}^2$	Acceleration variance over 10 s interval using 10 Hz acceleration

Table 3. Statistical model for computing the grid of posterior probabilities for trap camera locations.

Eq. No.	Model
Deployment location	
3.1	$\tilde{x}^{(i)} = x_{START}^{(i)} + \dfrac{n^{(i)}}{N^{(i)}}[x_{END}^{(i)} - x_{START}^{(i)}]$
3.2	$\tilde{y}^{(i)} = y_{START}^{(i)} + \dfrac{n^{(i)}}{N^{(i)}}[y_{END}^{(i)} - y_{START}^{(i)}]$
3.3	$\mu^{(i)} = [\tilde{x}^{(i)}, \tilde{y}^{(i)}]$
Grid cells	
3.4	$(j, k) \in \{-124, -123, \ldots, 124, 125\}^2$
3.5	$\Theta_{j,k}^{(i)} = [\tilde{x}^{(i)} + 10j, \tilde{y}^{(i)} + 10k]$
Likelihood grid	
3.6	$L_{j,k}^{(i)} = \mathcal{L}^{(i)}[\Theta_{j,k}^{(i)} \mid \hat{d}^{(i)}, \tau^2] = \dfrac{1}{\sqrt{2\pi\tau^2}} e^{-\frac{[b_{j,k}^{(i)} - \hat{d}^{(i)}]^2}{2\tau^2}}$
Prior grid	
3.7	$p_{j,k}^{(i)} = p[\Theta_{j,k}^{(i)} \mid \mu^{(i)}, \Sigma] = \dfrac{1}{2\pi\sqrt{|\Sigma|}} e^{-[\Theta_{j,k}^{(i)} - \mu^{(i)}]^T \Sigma^{-1}[\Theta_{j,k}^{(i)} - \mu^{(i)}]}$
Posterior grid	
3.8	$P_{j,k}^{(i)} = \dfrac{L_{j,k}^{(i)} \cdot p_{j,k}^{(i)}}{\sum\limits_{(j,k)} L_{j,k}^{(i)} \cdot p_{j,k}^{(i)}}$

Video clips of dragging and suspended traps provided lower and upper bounds for the drag window. The difference between the start and end times of the drag window was considered the maximum potential dragging time.

We estimated the distance that a trap is dragged along the bottom by multiplying the estimated drag time by the estimated hauling speed (H) for each set, which we used to approximate the speed at which traps drag along the bottom. Haul speed was calculated using depth and time measurements during gear retrieval while the trap is suspended in the water column between 600 and 200 m, i.e.:

$$H = \frac{(d_t < 600) - (d_t > 200)}{t_{600} - t_{200}}$$

where $d_t < 600$ and t_{600} are the first depth measurement and time, respectively, during the trap retrieval shallower than 600 m, and $d_t > 200$ and t_{200} are the last depth measurement and time, respectively, during the trap retrieval deeper than 200 m.
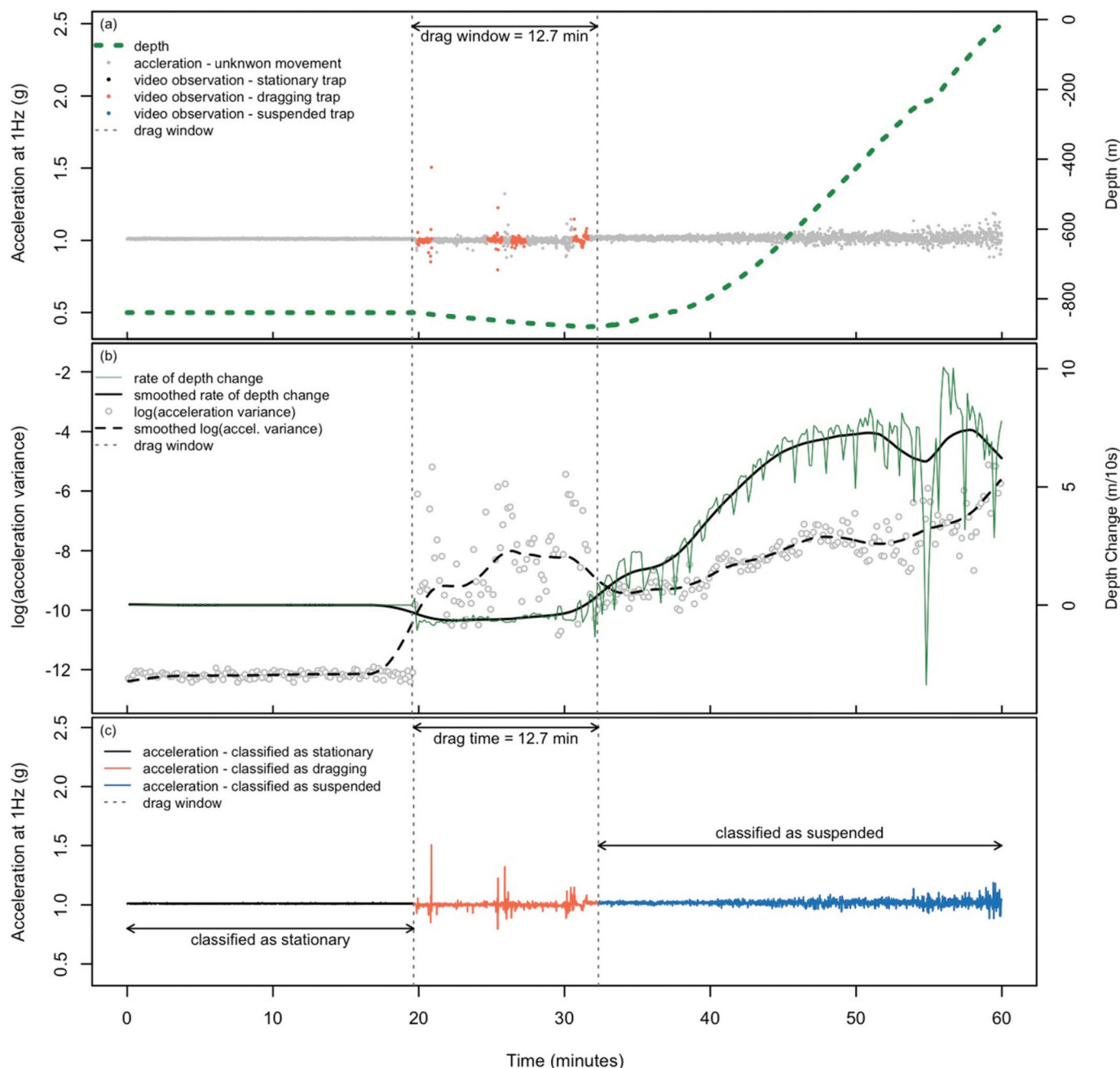
We estimated the possible furrow width created by a dragging trap by individually dragging 54-inch (1.37 m) bottom diameter sablefish traps along a sandy beach in five replicates of 5 m distance each (Fig. 6). Measurements of furrow width were taken at 0, 1, 2, 3, 4, and 5 m intervals along the tracks and averaged for each trial. The total bottom-contact area of traps during fishing was estimated by multiplying the mean drag furrow width by the estimated trap drag lengths for each set. An estimate of the bottom-contact area for a typical 60-trap set was then obtained by multiplying the trap bottom-contact area by 60 for each set.

Results

Direct observations of coral and sponge presence–absence

Deepwater corals or sponges were present at 26 locations and absent at 66 locations out of the 92 camera deployments that successfully obtained video of the bottom substrate at SK-B Seamount (Table 4; Fig. 7). Gorgonian corals (Order Alcyonacea) were the most commonly observed and diverse group, with at least six different species or taxonomic groups, including *Heteropolypus ritteri*, Isididae spp., *Paragorgia* spp., *Parastenella* sp., Primnoidae sp., and *Swiftia simplex*. We also observed sponges (Classes Demospongiae and Hexactinellida), seapens (Order Pennatulacea), hydrocorals (Family Stylasteridae), and black coral (Order Antipatharia) during camera deployments. The highest observed concentration of gorgonian corals was observed along the southwest and northeast flanks of the seamount. There were fewer locations with presence observations of sponges (7), sea whips (5), hydrocorals (3), and black corals (1) without any obvious consistency in their locations (Table 4; Fig. 7).

Fig. 4. Example of observations used to classify trap movement during the last hour of bottom longline trap fishing for a case where the trap is estimated to have dragged during the entire drag window (e.g., drag window = drag time). Raw accelerometer and depth data are shown in panels (*a*) and (*b*) and algorithm output for classifying trap movement in panel (*c*).

Here we only show trap camera observations in 2 km by 2 km grid cells due to privacy restrictions associated with commercial fishing data; however, the trap location estimator can provide higher spatial resolution for camera observations.
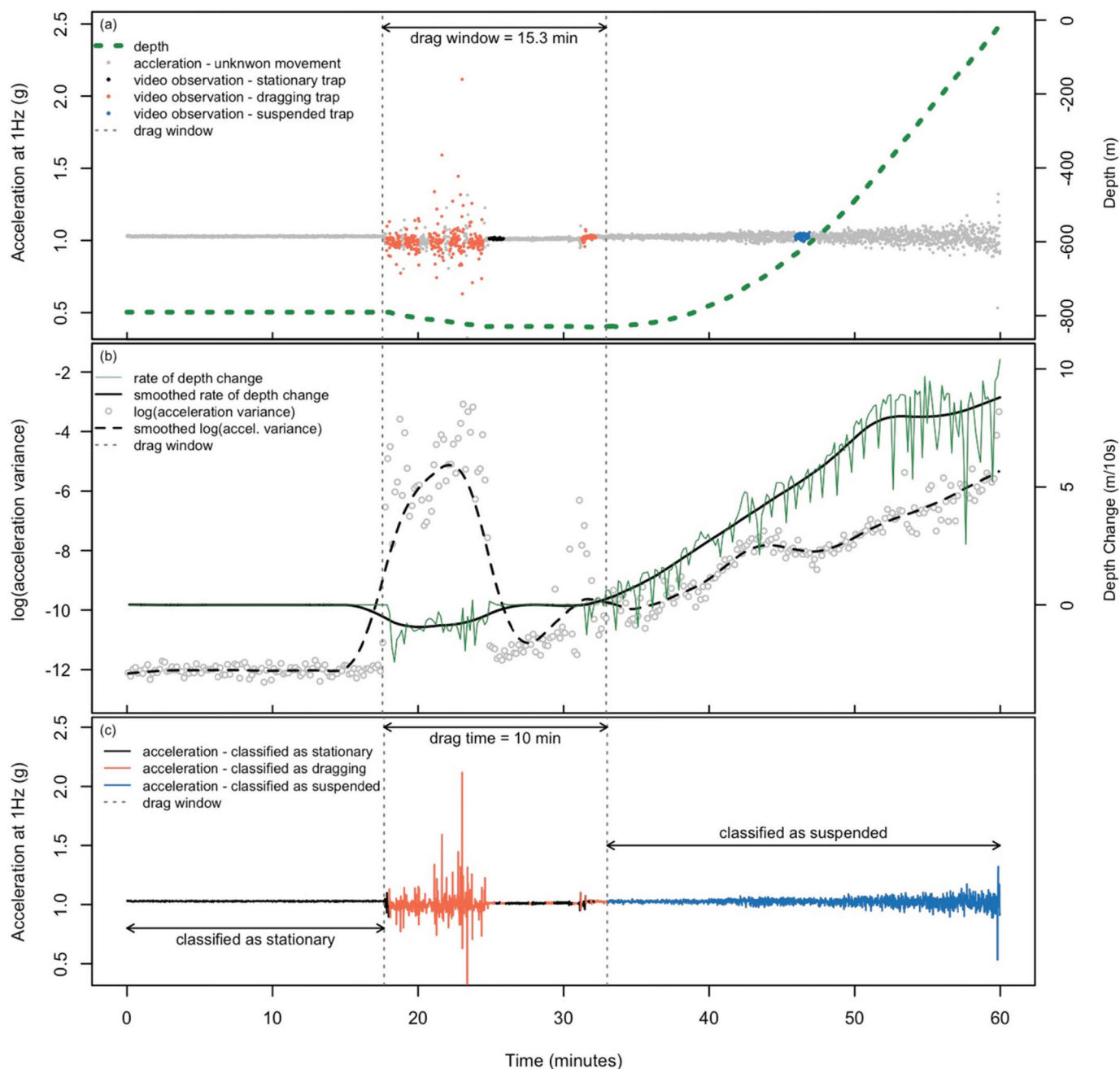
Trap location estimator

Figure 8 provides an example of the components involved in the posterior grid computation for estimating trap location on the bottom. Figure 8*a* shows the 10 m resolution multibeam bathymetry for a 1.25 km × 1.25 km area surrounding the initial trap deployment location along with the depth likelihood function grid (Fig. 8*b*) given by the observed depth at the trap bottom location. The depth likelihood is then combined with the spatial prior grid (only the prior mean is shown as the intersection of

dashed vertical and horizontal lines) to produce the final posterior grid (Fig. 8*c*), which in this case shows approximately 100 m northward displacement of the trap from its deployment location at the surface. Closer inspection of the posterior grid (Fig. 8*d*) shows that the posterior medoid location is on the very edge of the probability space, while the posterior mode lies within a larger region of reasonably high probability.

All three methods of estimating displacement from the deployment location are unimodal and highly left-skewed with an outlier at approximately 1200 m (Fig. 9). Based on the posterior mean estimator, expected displacement from the deployment location was greater than 200 m for all sets (median = 388 m; Fig. 9*a*), due to ridges of high likelihood extending along contours with the

Fig. 5. Example of observations used to classify trap movement during the last hour of bottom longline trap fishing for a case where the trap is estimated to have been stationary for multiple intervals during the drag window (e.g., drag window ≠ drag time). Raw accelerometer and depth data are shown in panels (*a*) and (*b*) and algorithm output for classifying trap movement in panel (*c*).
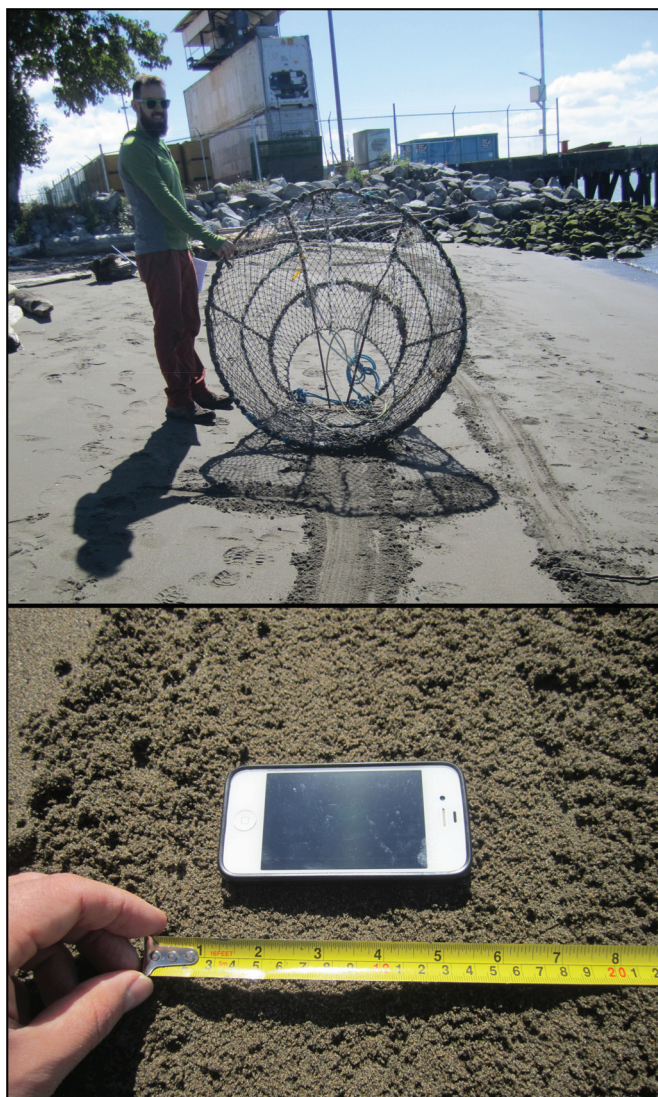
correct depth (see Fig. 8*b*). Displacements derived from the posterior mode estimator were closer to the surface deployment location (median = 203 m; Fig. 9*b*), while those derived from posterior medoids were in between the mean and mode (median = 265 m; Fig. 9*c*). Uncertainty in displacement from deployment locations, measured as squares that capture 50% of the posterior density, have side lengths of 430 m based on the modes and 390 m based on posterior medoids, while squares that capture 95% of the posterior density have side lengths of 1190 m (mode) and 1150 m (medoid).

The maximum probability of a camera trap landing in a single 10 m × 10 m square cell ranged from 0.6% to 4.6% across all 99 sets. Depth of the set was not correlated with the distance from deployment (Pearson R^2 < 0.2 based on posterior medoids).

Bottom-contact area

The results from the classification of trap movement and estimates of bottom-contact area are shown in Fig. 10 and Table 5. These statistics exclude one set where the trap was wedged in a rock crevice that prevented any trap movement during retrieval, because this behaviour was not observed in any of the other 92 sets with video observations. The estimated drag window and drag time for the excluded set were 5.9 min and 0.4 min, respectively. The mean estimated bottom-contact area for a 54-inch trap was 53 m² (95% CI = 40–65 m²), which is nearly 36 times the static trap footprint of 1.47 m² (i.e., the bottom area of the trap). Variability in the estimated drag times and drag lengths dominated bottom area calculations compared with less variable haul speeds and drag widths (Fig. 10).

Fig. 6. Drag paths (top) created by dragging a sablefish commercial trap with 54-inch (1.37 m) bottom diameter along a sandy beach and example path width measurement (bottom).

The start of the drag window is indicated by an increase in the acceleration variance and increased magnitude of depth change (Figs. 4, 5). As gear retrieval continues, there is a noticeable decrease in depth until eventually the trap moves vertically off the bottom and becomes suspended in the water column (e.g., the end of the drag window). When this occurs, there is usually a decrease in acceleration variance and a positive increase in the rate of depth change (Figs. 4, 5).

Video observations, depth, and accelerometer data indicate that traps do not always drag continuously (Fig. 5) and that traps can start and stop dragging frequently during gear retrieval. The stationary intervals during the drag window were classified as such when the rate of depth change for a 10 s interval was zero (Step 2). This step of the classifying algorithm is important since deviations between the drag window and the estimated drag time can be substantial (Fig. 11). The estimated mean drag window (i.e., the period in which there is potential for the gear to drag along the seafloor) was 1.25 times longer than the estimated mean drag time (Table 5). The maximum difference between the drag window and drag time estimates was 9 min, where the drag window was nearly 2.9 times longer than the estimated drag time. If the drag window was used in the bottom footprint calculation, the

mean footprint would be 4000 m² instead of the 3200 m² calculated using the estimated drag time, which would overestimate the contact area.

Video observations from trap cameras deployed at SK-B and during the sablefish survey confirm that the polypropylene groundline remains suspended off the bottom; however, because the trap camera field of view is pointed at the substrate, there are limited groundline observations. The groundline is only visible when traps land upside down or are rotated during gear retrieval to allow a camera view of the water column and space above the traps. There were 33 sets at SK-B where the groundline could be viewed while under tension off the bottom when traps were moving along the seafloor. Note that these videos only provide a view of a small portion of the groundline that is directly above the trap.

Discussion

Contemporary fisheries are increasingly challenged to improve conservation of both fish stocks and essential habitats as part of government and ecocertification requirements (DFO 2010; Furness et al. 2010; Heupel and Auster 2013). Fisheries in Canada will also need to adapt to a growing number of MPA closures. The Government of Canada recently reaffirmed commitments to protect 10% of coastal and marine waters by 2020 as part of the Aichi Biodiversity Targets, with plans to implement half this area by 2017. For habitat conservation, in particular, we lack the detailed knowledge about distribution, composition, vulnerability, and habitat productivity necessary to effectively protect important deepwater habitats. In this paper, we demonstrate how a collaborative academic–industry–government approach to studying deepwater ocean habitats and the risks posed by longline trap fishing gear could provide an improvement in our ability to design and implement protections for sensitive benthic habitats. In particular, we obtained (*i*) high-quality presence–absence observations for corals and sponges over a large area within the SK-B Seamount MPA and (*ii*) direct video observations of trap interactions with the seafloor, which we combined with accelerometer and depth sensors to develop an algorithm for estimating the bottom-contact area of longline trap gear.

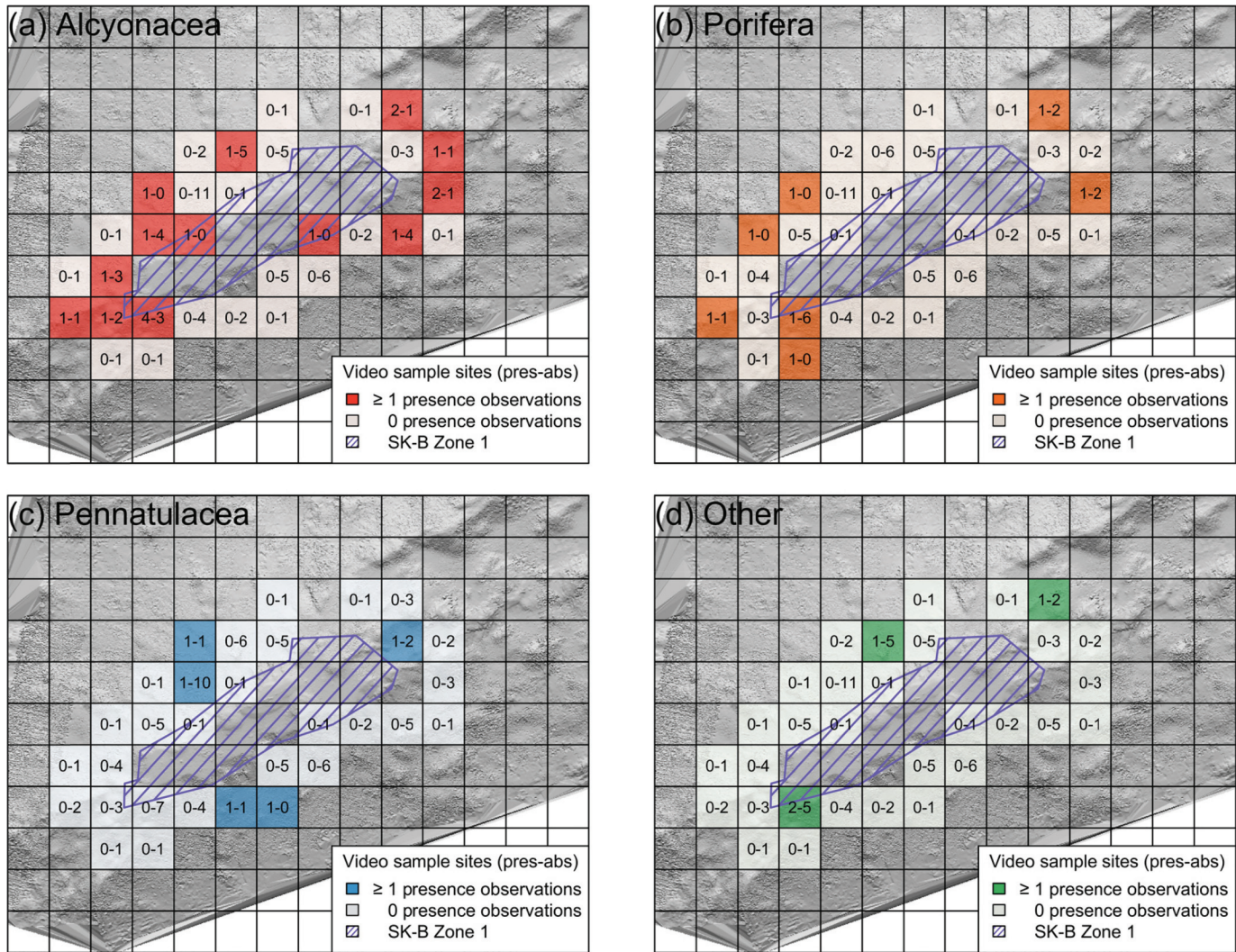### Understanding bottom-contact area of longline trap gear

Video observations and accelerometer measurements confirm that sablefish traps are typically stationary once the gear has settled on the bottom and that the main interaction with the seafloor occurs by traps over a short window of time when traps drag along the bottom during the gear retrieval. For the fishing sets analysed at SK-B, gear retrieval usually begins at the deep end of the set, and the short period of increasing depth sensor measurements observed during the drag window suggest that traps initially drag in the downslope direction during hauling. Video and accelerometer data also indicate that traps start and stop dragging frequently during gear retrieval, presumably because of stoppages to remove catch as traps reach the surface.

Our trap location estimator allows relatively accurate mapping of the fishing effort distribution on the seafloor, as well as the footprint within or near sensitive benthic habitats. Such information could be used to quantitatively determine longline trap gear footprints at the relatively fine-scale resolution needed to inform coral and sponge risk assessments at SK-B. The distribution of distances between deployment locations and estimated landing positions also provides valuable information that can be used to determine the appropriate area and buffers for closures designed to protect sensitive habitats. Delineating borders and different zoning for conservation areas in Canada can occur on a scale of 100–1000 m for many smaller-scale (e.g., 0.6–475 km²) fishery closures designed to protect sponge (e.g., Hecate Strait – Queen Charlotte Sound Glass Sponge Reefs MPA, Strait of Georgia Glass Sponge Reef Closures, Sambro Bank, Emerald Basin) and coral habitats (e.g., Northeast Channel Coral Conservation Area, Lophelia Coral Conser-

806

Can. J. Fish. Aquat. Sci. Vol. 75, 2018

Table 4. Presence (P) and absence (A) frequencies by sampling year and total frequencies and percentages over all years from 92 video sample sites during May 2013–2015 sablefish fishing trips at SK-B Seamount.

Observations	2013 P–A	2014 P–A	2015 P–A	2013–2015 P–A	%P	%A
Gorgonian corals (Order Alcyonacea)	3–9	9–45	6–20	18–74	20	80
Sponges (Phylum Porifera)	4–8	3–51	0–26	7–85	8	92
Sea whips (Order Pennatulacea)	1–11	2–52	2–24	5–87	5	95
Hydrocorals (Family Stylasteridae)	1–11	2–52	0–26	3–89	3	97
Black corals (Order Antipatharia)	1–11	0–54	0–26	1–91	1	99
Corals or sponge	6–6	12–42	8–18	26–66	28	72

Fig. 7. Presence–absence (pres–abs) video sample sites in 2 km × 2 km grid cells for (*a*) Alcyonacea, (*b*) Porifera, (*c*) Pennatulacea, and (*d*) Other (Antipatharia or Stylasteridae) from trap camera deployments during May 2013–2015 fishing trips at SK-B. The dark-coloured cells are grid cells with presence observations during at least one camera deployment in that cell, while light-coloured cells indicate that the specified taxa was absent (i.e., 0 presence observations) for all video samples within that cell. Numbers indicate video sampling sites in the grid cell with presence and absence observations (pres–abs). For example, a value of 1-2 in panel (*a*) indicates one video sample site where Alcyonacea was present and two video sample sites where Alcyonacea was absent.
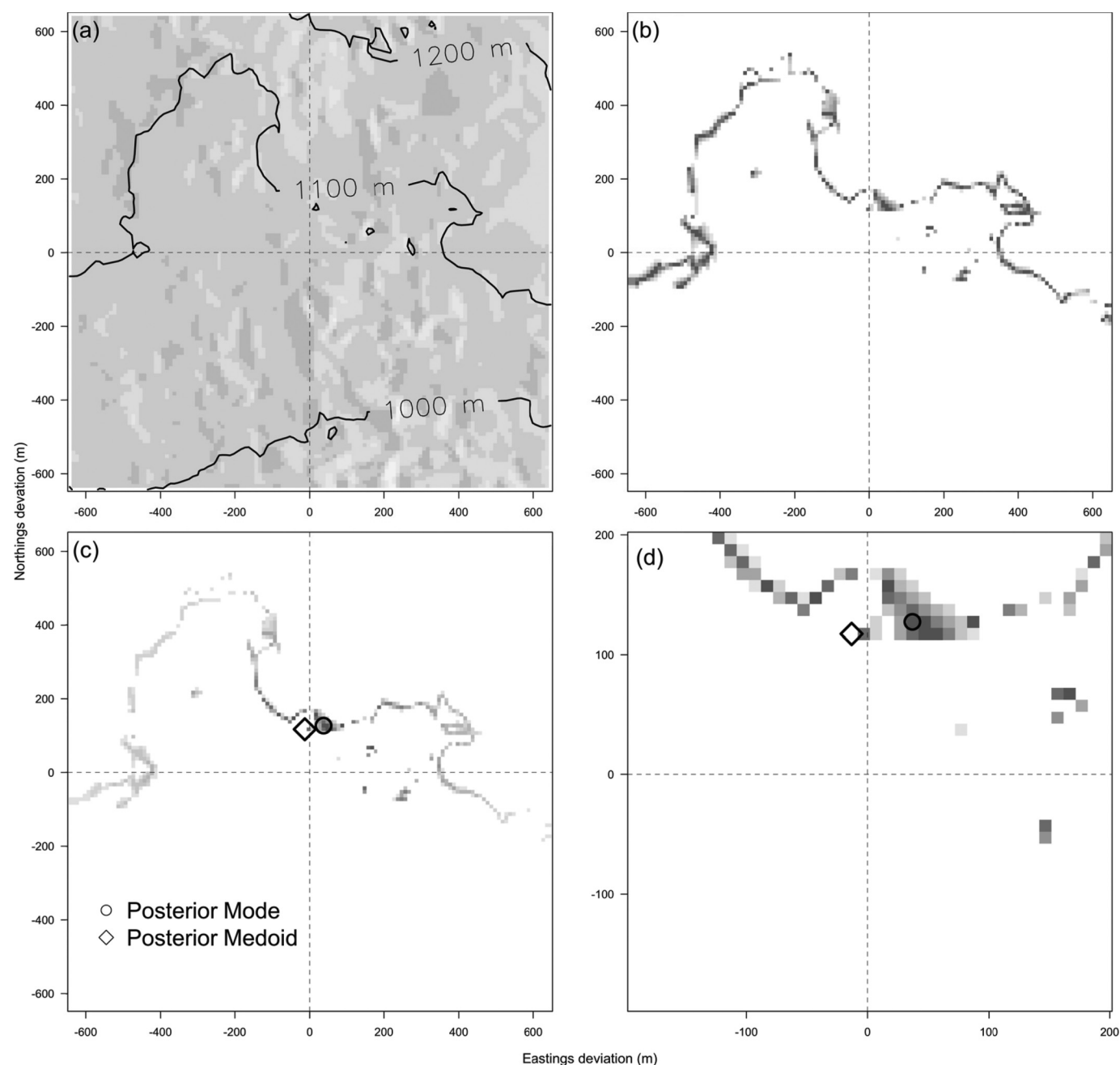

vation Area, The Gully MPA, SK-B Seamount MPA Zone 1). Inaccurate spatial mapping and inappropriate buffer sizes in these kinds of closures may unnecessarily reduce fishing opportunities or reduce the effectiveness of closures designed to protect SBAs.

Estimates in this study are from a small sample size of fishing trips at SK-B Seamount; trap footprint and deployment distances may differ for other fishing vessels, fishing conditions, and fishing areas on the coast. For instance, the outlier displacement estimate of 1200 m from the deployment location may be the result of towing the gear or high currents during trap deployment. Further experiments under different fishing conditions will likely improve our ability to estimate how different environmental condi-

Fig. 8. Trap location estimator components for a single set of traps: (*a*) 1.25 km by 1.25 km subset of the multibeam bathymetry grid, (*b*) the depth likelihood function, (*c*) the Bayes posterior grid, and (*d*) a zoomed 0.4 km by 0.4 km subset of panel (*c*). Intersection of the dashed lines indicates the prior mean location based on the estimated deployment location ($\tilde{x}$, $\tilde{y}$). Shading in panels (*b*), (*c*), and (*d*) indicates likelihood or probability density, with darker cells indicating higher density. Panels (*c*) and (*d*) indicate the posterior mode (circle) and medoid (diamond) trap location estimates.
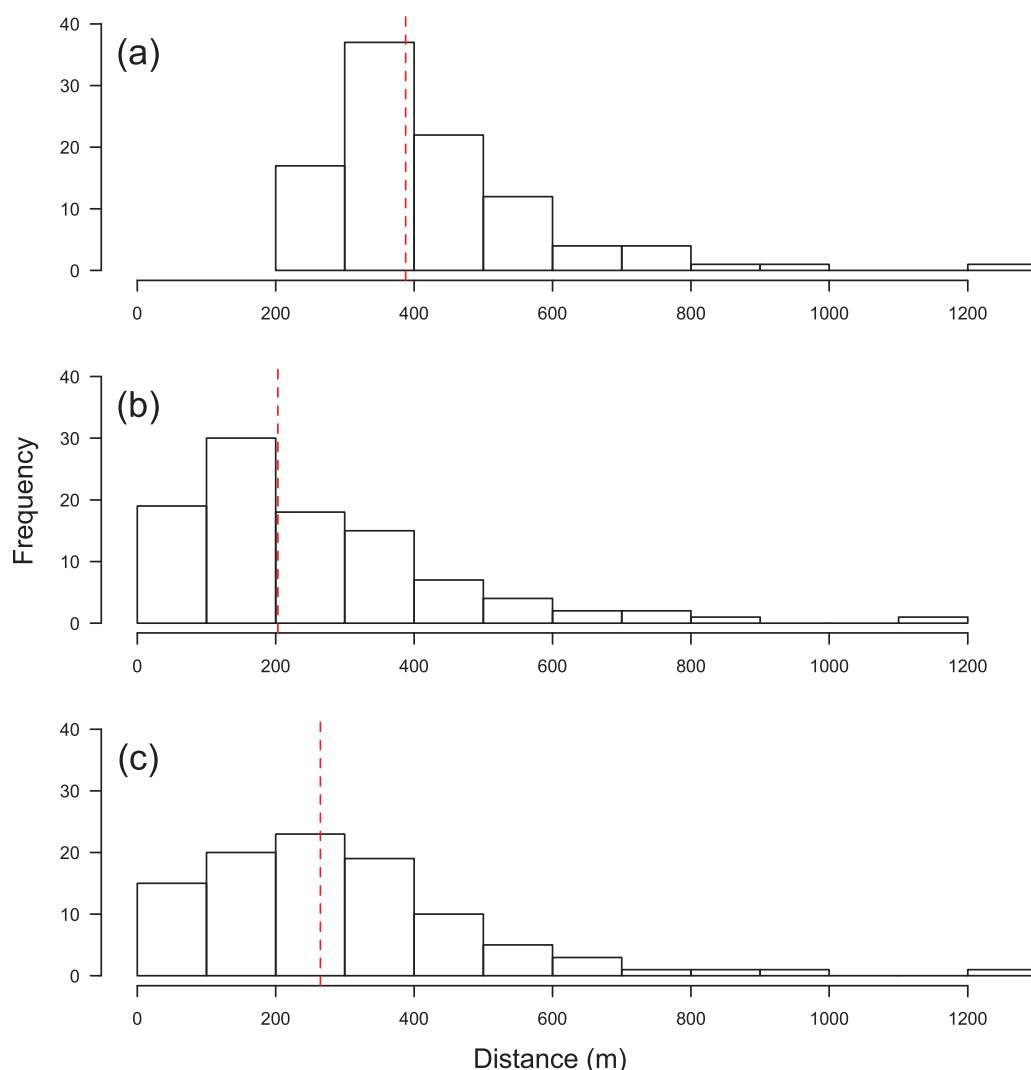

tions and fishing characteristics influence gear displacement from drop locations, as well as different gear behaviour during retrieval. As part of that work, upgrades to our camera systems could automatically obtain GPS location data for the vessel at the trap camera deployment and surface retrieval rather than using crude start and end deployment locations in the Bayesian spatial prior distributions.

Our approach to estimating gear movement can be adapted to other types of bottom longline fisheries (e.g., longline hook and other trap gear and bottom trawls). This will allow a quantitative assessment of the cumulative impacts and comparison of footprints from different bottom-contact fisheries in overlapping areas (Welsford et al. 2014*a*). For example, our mean estimate of the footprint for a 60-trap longline sablefish set (3200 m²) is 6% of the mean footprint estimates for bottom longline hook sets (55 000 m²) in the Heard Island and McDonald Islands off Antarctica, based on a footprint width of 6.2 m and mean set length of 8.9 km (Ewing and Kilpatrick 2014; Welsford et al. 2014*a*). Estimates of footprint widths do not exist for the different British Columbia longline hook fisheries (Fig. 1), and set lengths are shorter with median lengths of 3.0, 2.6, 2.4, and 1.8 km for sets during 2006–2011 in the sablefish trap and halibut, Schedule II, and ZN longline hook fisheries, respectively (data from DFO groundfish database archived at the Pacific Biological Station in

Fig. 9. Empirical distributions (*n* = 99 sets) of three estimates of the posterior (*a*) mean, (*b*) mode, and (*c*) medoid distance from the estimated deployment location of camera traps. The dashed lines indicate the median values of each distribution.

Nanaimo, British Columbia). Bottom trawl footprint estimates vary based on the width of the trawl net and the length of the tow and are much larger than longline hook and trap footprints. The mean trawl footprints per fishing event estimated by Welsford et al. (2014*a*) ranged from 295 000 to 1 134 000 m² for four different vessels, based on footprint widths ranging from 100 to 160 m and mean tow lengths ranging from 2.9 to 7.6 km. Other metrics can also be used to compare the bottom impacts of different fishing gear, such as the footprint per hour of fishing (Eigaard et al. 2016) or catch per square metre of bottom contact.

Our analysis focused on measuring the bottom-contact area of traps, as our observations indicate this is the largest contributor to total bottom-contact area of sablefish longline trap fishing gear. The two anchors at terminal set ends are also in contact with the bottom (Fig. 2), and there is potential for occasional groundline bottom contact, but the footprint of these gear components is considered small relative to the trap footprint. There were two 1 min video clips where the groundline was observed in close proximity to the bottom, suggesting that it is possible that the groundline may occasionally contact the bottom or entangle larger free-standing structures in certain fishing conditions (e.g., in areas with high rugosity or steep bathymetry), although this was not observed. Given the large variability in trap footprint estimates for different sets,

there may be marginal benefits to quantifying anchor and groundline bottom contact for this particular gear.

Longline trap gear used in the British Columbia sablefish fishery appears to have properties that result in smaller footprints in comparison with other longline hook and trap gears. For example, as confirmed by video observations, extruded polypropylene groundline on sablefish trap gear is buoyant even at extreme depths and rarely contacts the seafloor. Lack of bottom contact means that lateral movement of the groundline during retrieval is less likely to cause damaging shearing effects along the bottom as observed for groundlines used in longline hook fisheries (Ewing and Kilpatrick 2014). In addition, conical traps with a circular base create narrower furrow widths during dragging compared with a square trap base of the same total area. The trap bridle connection at the top of a sablefish trap causes traps to drag on their sides during retrieval resulting in a footprint width during dragging that is much less than the trap bottom diameter. In contrast, observed contact area created by box-shaped King crab pots on longlines in Alaska had widths ranging from 2 to 9 m (Stone 2006) for 2.4 m × 2.4 m pots. We measured furrow widths created by dragging traps on a beach with wet sand to simulate the drag paths created during fishing operations; however, in situ observations of furrow widths could be obtained via video using camera

Fig. 10. Distributions (*n* = 20 sets) of (*a*) estimated drag times of camera traps, (*b*) mean haul speed between 200 and 600 m depths for camera traps, (*c*) estimated drag lengths for camera traps, and (*d*) estimated bottom-contact areas for a 60-trap bottom longline set using a mean drag width of 17.0 cm (SE 0.8 cm).
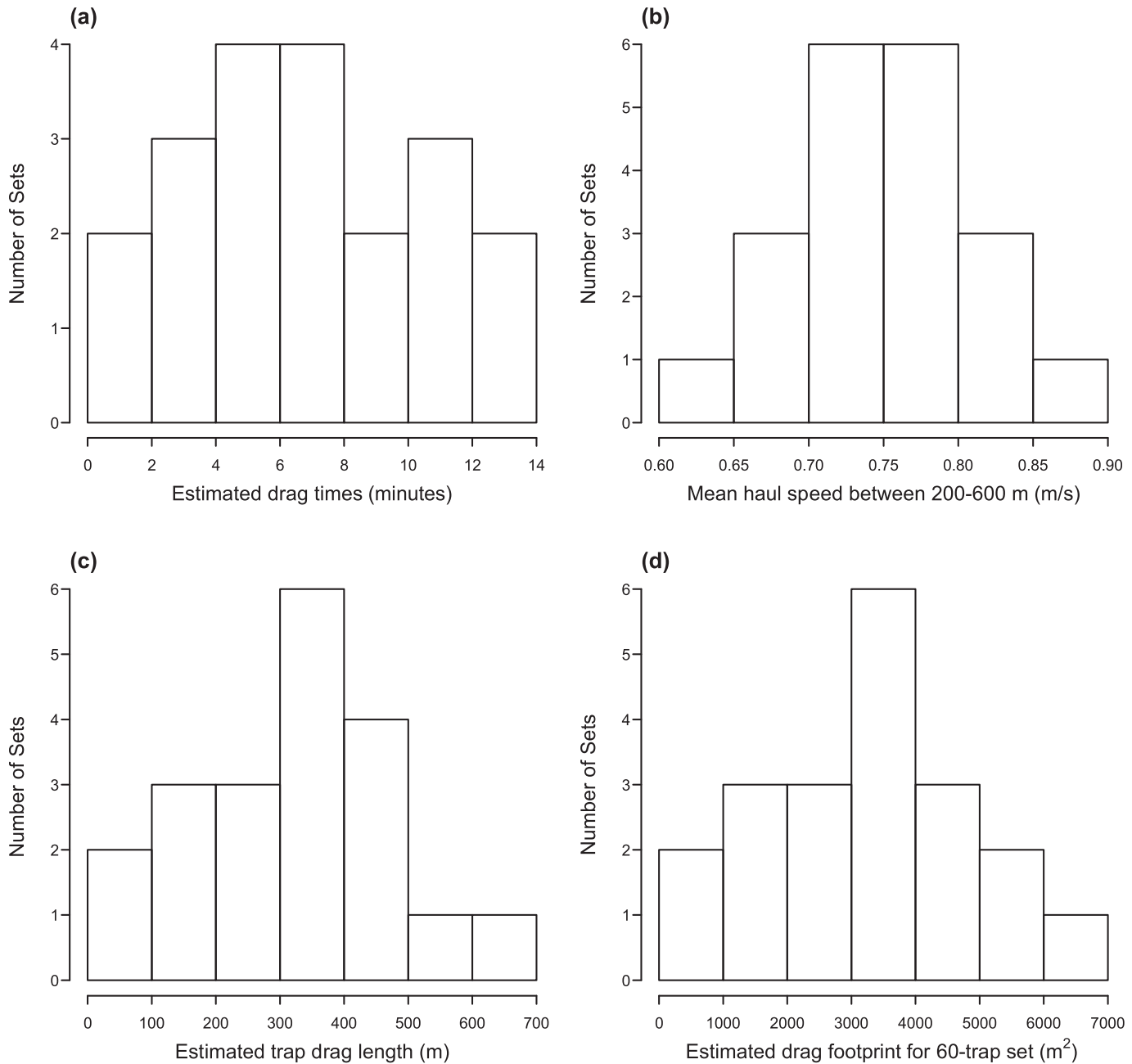

Table 5. Summary statistics for trap movement and bottom-contact area estimates from longline trap fishing sets at SK-B Seamount in 2015.

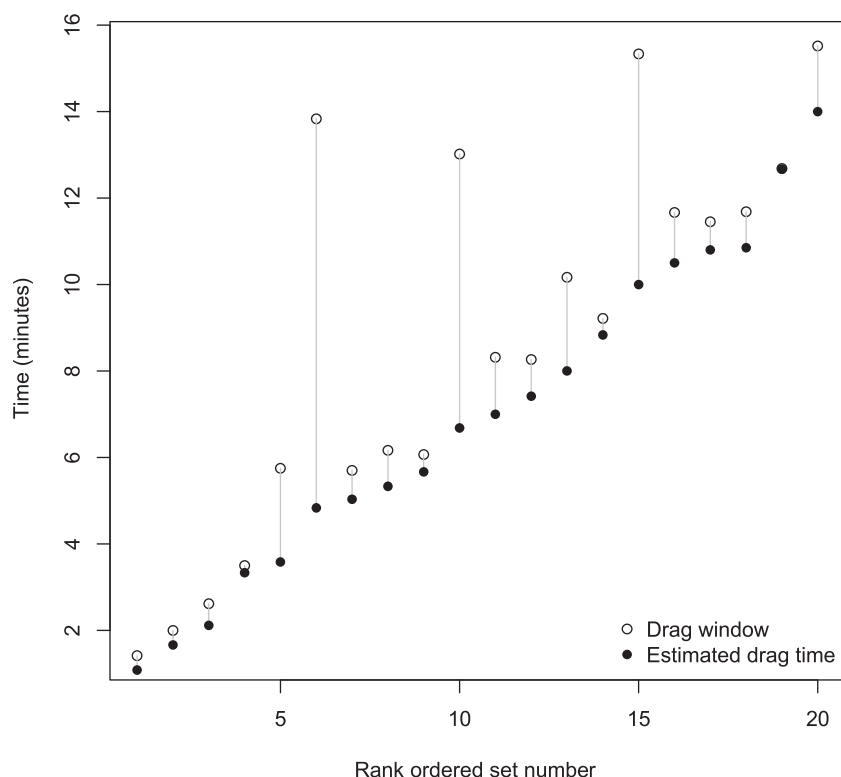| Metric	Mean	95% CI	Range
Drag window (min)	8.72	6.65–10.79	1.42–15.52
Drag time (min)	6.97	5.23–8.71	1.08–14.00
Haul speed (m·s⁻¹)	0.75	0.72–0.78	0.64–0.89
Drag length (m)	310	238–383	44–610
Drag path width (m)	0.17	0.15–0.19	0.15–0.20
Single trap footprint (m²)	53	40–65	7.4–104
Footprint for 60-trap set (m²)	3200	2400–3900	400–6200

Note: *n* = 5 for path width estimates and 20 for all other statistics.

configurations that provide unobstructed views of fishing gear (see Kilpatrick et al. 2011) or via scuba diving alongside traps retrieved in shallower water.

Next steps: understanding risks to seafloor habitats

The first two steps in evaluating specific fishery risks to deep-sea bottom habitats are (*i*) collecting data to map the locations of sensitive benthic areas and (*ii*) calculating the seafloor area that is contacted by fishing gear. In this study, we have described the methods and ongoing data collection that can provide this information by generating high-resolution habitat suitability maps and estimating the historical fishing footprint at SK-B. Additional information such as estimates of fishing mortality and recovery rates from damage, as well as methods to mitigate bottom contact, are also important, but beyond the scope of this paper.

810

Can. J. Fish. Aquat. Sci. Vol. 75, 2018

Fig. 11. Classified drag window (i.e., period where there is potential for dragging) and estimated drag times for 20 sets. Sets rank number is ordered by increasing drag time estimates. Set numbers 19 and 15 correspond with sets shown in Figs. 4 and 5, respectively.

The trap location estimates provide more accurate coordinates for camera observations that can improve species distribution modelling. This is important because accurate mapping of SBAs will increase the effectiveness of management measures designed to protect bottom habitats and can reduce lost fishing opportunities arising from large-scale fishing closures that include areas that may not actually contain SBAs. Typical species distribution models extract predictor variables from existing environmental data or oceanographic models (Rooper et al. 2014; Lagasse et al. 2015) based on the position of the observation even though there can be considerable uncertainty for observations collected during fishing activities. For example, the potential location of coral and sponge bycatch can span several kilometres for data collected during bottom trawling. For the trap camera-based observations, the posterior mode or medoid estimates of trap locations provide the best location estimates given the data available and can allow for more relevant selection of predictor variable locations used in model fitting. As an alternative to using a single grid cell as a point estimate of locations, the posterior density also provides a probability distribution that can be used to weight multiple grid cells when extracting predictor data from environmental raster layers.

Risks to habitat are not only influenced by the amount of gear that is deployed per year and the frequency that specific areas are contacted, but also by the cumulative effects over multiple fishing years and the recovery rates during the time between subsequent contact events (Constable 2014). Our bottom footprint estimates can be used to identify potential at-risk SBAs within the SK-B Seamount MPA where high historical fishing intensity overlaps with areas of high probability for coral or sponge presence. For instance, we could use the historical trap deployment locations at SK-B along with the estimated contact area for each trap to estimate the frequency and cumulative trap gear contact for each patch of seafloor. Thus, the next step in understanding fishing bottom impacts is to estimate the mortality rate or damage to coral or sponge populations that occurs when fishing gear lands

in a specific area, as well as recovery rates from fishing damage. For example, Ewing et al. (2014) estimated the probability that individuals or colonies within the bottom-contact area of different fishing gears would experience no damage, sublethal damage, or lethal damage, based on a variety of data sources such as life history, morphology, and in situ observations. Both High (1998) and Eno et al. (2001) observed cases where flexible corals bent during contact with traps and longlines and showed no apparent damage. Nonlethal damage such as lesions to gorgonian coenenchyme can allow for full recovery; however, in some cases it may also increase the probability of lethal damage from future fishing events (Bavestrello et al. 1997; Ewing et al. 2014). Different species or groups of species will also have different recovery rates from fishing damage. Rooper et al. (2011) estimated intrinsic growth rates for corals and sponges in the Aleutian Islands were slow and that recovery from a large mortality of biomass could take several decades. More detailed studies on the life history of specific coral and sponge species that occur in SK-B could reduce parameter uncertainty and improve our ability to assess fishing risks to these habitats.

Our approach to estimating the bottom footprint of longline trap gear provides a method to estimate and compare the bottom-contact area of different fishing events, which, in turn, can be used to evaluate strategies aimed at minimizing fishing footprints and risks to SBAs. For example, it is likely that certain fishing characteristics (e.g., hauling speed, haul direction, catch, crew experience) combine with environmental conditions (e.g., depth, slope, rugosity, current, wind) to affect the size of the trap footprint. Thus, direct estimates of the fishing footprint can provide the data needed to test how alternative gear modifications (e.g., trap numbers, trap size, trap shape, bridle connections, groundline material) and hauling procedures could reduce bottom impacts. In this study, we only examined traps deployed in the middle of the set, assuming the same footprint applied over the

full set; however, it may be that traps at either end of the string may drag more or less than traps located in the middle.

Future research could deploy cameras, accelerometers, and depth sensors on multiple traps along the set to improve footprint estimates and understanding of gear behaviour. Furthermore, the small size and relatively low expense accelerometers (e.g., US$100–US$250) could be deployed much more broadly on commercial fishing sets to capture a wider range of gear behaviour.

Conclusion

The deployment of cameras and motion-sensing equipment on commercial fishing gear, such as sablefish traps, can provide regular observations of biological communities on the seabed as well as the information needed to estimate the bottom footprint of the gear. These direct observations provide valuable information needed to investigate strategies for reducing risks to sensitive bottom habitats, while still allowing fisheries access to valuable fishing grounds. Advances in technology and miniaturization create massive potential to expand this approach to larger spatial scales, which would allow greater fishing industry contributions toward mapping sensitive benthic areas and informing ecosystem-based management.

Acknowledgements

References

Austin, W.C., Ott, B.S., Reiswig, H.M., Romagosa, P., and McDaniel, N.G. 2013. Two new species in the family Axinellidae (Porifera, Demospongiae) from British Columbia and adjacent waters. ZooKeys, **338**: 11–28. doi:10.3897/zookeys.338.5535.

Bavestrello, G., Cerrano, C., Zanzi, D., and Cattaneo-Vietti, R. 1997. Damage by fishing activities to the Gorgonian coral *Paramuricea clavata* in the Ligurian Sea. Aquat. Conserv. **7**(3): 253–262. doi:10.1002/(SICI)1099-0755(199709)7:3<253::AID-AQC243>3.0.CO;2-1.

Bo, M., Bava, S., Canese, S., Angiolillo, M., Cattaneo-Vietti, R., and Bavestrello, G. 2014. Fishing impact on deep Mediterranean rocky habitats as revealed by ROV investigation. Biol. Conserv. **171**: 167–176. doi:10.1016/j.biocon.2014.01.011.

Buhl-Mortensen, L., Vanreusel, A., Gooday, A.J., Levin, L.A., Priede, I.G., Buhl-Mortensen, P., Gheerardyn, H., King, N.J., and Raes, M. 2010. Biological structures as a source of habitat heterogeneity and biodiversity on the deep ocean margins. Mar. Ecol. **31**: 21–50. doi:10.1111/j.1439-0485.2010.00359.x.

Cairns, S.D. 2007. Calcaxonian Octocorals (Cnidaria: Anthozoa) from Eastern Pacific Seamounts. Proc. Calif. Acad. Sci. **58**: 511–541.

Clark, M.R., Althaus, F., Schlacher, T.A., Williams, A., Bowden, D.A., and Rowden, A.A. 2016. The impacts of deep-sea fisheries on benthic communities: a review. ICES J. Mar. Sci. **73**(s1): i51–i69. doi:10.1093/icesjms/fsv123.

Collie, J.S., Hall, S.J., Kaiser, M.J., and Poiner, I.R. 2000. A quantitative analysis of fishing impacts on shelf-sea benthos. J. Anim. Ecol. **69**(5): 785–798. doi:10.1046/j.1365-2656.2000.00434.x.

Constable, A. 2014. A simulation model for evaluating management strategies to conserve benthic habitats (vulnerable marine ecosystems) which are potentially vulnerable to impacts from bottom fisheries. *In* Demersal fishing interactions with marine benthos in the Australian EEZ of the Southern Ocean: an assessment of the vulnerability of benthic habitats to impact by demersal gears. *Edited by* D.C. Welsford, G.P. Ewing, A.J. Constable, T. Hibberd, and R. Kilpatrick. Australian Antarctic Division. pp. 247–255.

DFO. 2005. Canada's federal marine protected areas strategy. Fisheries and Oceans Canada, Ottawa, Ont.

DFO. 2010. Pacific region cold-water coral and sponge conservation strategy 2010–2015. Oceans Program, Fisheries and Oceans Canada, Vancouver, B.C.

DFO. 2015. Sablefish Commercial Harvest Plan. *In* Pacific Region Groundfish Integrated Fisheries Management Plan. Version 1.3. pp. 1–25, appendix 7.

Doherty, B., and Cox, S. 2017. Data summary of trap camera video obtained during Sablefish bottom longline trap fishing at SGaan Kinghlas – Bowie Seamount, 2014–2015. Can. Dat. Rep. Fish. Aquat. Sci. 1276. Fisheries and Oceans Canada.

Durán Muñoz, P., Murillo, F.J., Sayago-Gil, M., Serrano, A., Laporta, M., Otero, I., and Gómez, C. 2011. Effects of deep-sea bottom longlining on the Hatton Bank fish communities and benthic ecosystem, north-east Atlantic. J. Mar. Biol. Assoc. U.K. **91**(4): 939–952. doi:10.1017/S0025315410001773.

Eigaard, O.R., Bastardie, F., Breen, M., Dinesen, G.E., Hintzen, N.T., Laffargue, P., Mortensen, L.O., Nielsen, J.R., Nilsson, H.C., O'Neill, F.G., Polet, H., Reid, D.G., Sala, A., Skold, M., Smith, C., Sorensen, T.K., Tully, O., Zengin, M., and Rijnsdorp, A.D. 2016. Estimating seabed pressure from demersal trawls, seines, and dredges based on gear design and dimensions. ICES J. Mar. Sci. **73**(s1): i27–i43. doi:10.1093/icesjms/fsv099.

Eno, N.C., MacDonald, D.S., Kinnear, J.A., Amos, S.C., Chapman, C.J., Clark, R.A., Bunker, F.S.P., and Munro, C. 2001. Effects of crustacean traps on benthic fauna. ICES J. Mar. Sci. **58**: 11–20. doi:10.1006/jmsc.2000.0984.

Ewing, G., and Kilpatrick, R. 2014. Estimating the gear footprint of demersal trawl and longline fishing gears used in the Heard Island and McDonald Islands fisheries. *In* Demersal fishing interactions with marine benthos in the Australian EEZ of the Southern Ocean: an assessment of the vulnerability of benthic habitats to impact by demersal gears. *Edited by* D.C. Welsford, G.P. Ewing, A.J. Constable, T. Hibberd, and R. Kilpatrick. Australian Antarctic Division. pp. 176–198.

Ewing, G., Hibberd, T., and Welsford, D. 2014. Assessing the resistance of vulnerable benthic taxa to disturbance from demersal fishing in the HIMI region. *In* Demersal fishing interactions with marine benthos in the Australian EEZ of the Southern Ocean: An assessment of the vulnerability of benthic habitats to impact by demersal gears. *Edited by* D.C. Welsford, G.P. Ewing, A.J. Constable, T. Hibberd, and R. Kilpatrick. Australian Antarctic Division. pp. 226–245.

Furness, R., Knapman, P., Nichols, J., and Scott, I. 2010. MSC assessment report for the Canadian Pacific Sablefish (*Anoplopoma fimbria*) fishery. Moody International.

Government of Canada. 2014. Canada–British Columbia marine protected area network strategy.

Halcro, K. 2000. July/August trip report: Pacific report, NOAA Ship Rainier, Kodiak Island area, Bowie & Hodgkins seamounts. Canadian Hydrographic Service, Department of Fisheries and Oceans, Institute of Ocean Sciences, Sidney, B.C.

Hastie, T., and Fithian, W. 2013. Inference from presence-only data; the ongoing controversy. Ecography, **36**: 864–867. doi:10.1111/j.1600-0587.2013.00321.x. PMID:25492992.

Heifetz, J., Stone, R.P., and Shotwell, S.K. 2009. Damage and disturbance to coral and sponge habitat of the Aleutian Archipelago. Mar. Ecol. Prog. Ser. **397**: 295–303. doi:10.3354/meps08304.

Heupel, E., and Auster, P.J. 2013. Eco-labeling seafood: Addressing impacts to vulnerable seafloor species, communities, habitats and ecosystems in data-poor regions. Mar. Pol. **38**: 8–15. doi:10.1016/j.marpol.2012.05.014.

High, W.L. 1998. Observations of a scientist/diver on fishing technology and fisheries biology. Alaska Fisheries Science Center Processed Report 98-01, National Marine Fisheries Service, National Oceanic Atmospheric Administration, Seattle, Wash.

Hourigan, T. 2009. Managing fishery impacts on deep-water coral ecosystems of the USA: emerging best practices. Mar. Ecol. Prog. Ser. **397**: 333–340. doi:10.3354/meps08278.

Hourigan, T.F., Lumsden, S.E., Dorr, G., Bruckner, A.W., Brooke, S., and Stone, R.P. 2007. Deep coral ecosystems of the United States: Introduction and national overview. *In* The state of deep coral ecosystems of the United States. *Edited by* S.E. Lumsden, T.F. Hourigan, A.W. Bruckner, and G. Dorr. NOAA Tech. Memo CRCP-3. pp. 1–64.

Kaiser, M.J., Clarke, K.R., Hinz, H., Austen, M.C.V., Somerfield, P.J., and Karakassis, I. 2006. Global analysis of response and recovery of benthic biota to fishing. Mar. Ecol. Prog. Ser. **311**: 1–14. doi:10.3354/meps311001.

Kilpatrick, R., Ewing, G., Lamb, T., Welsford, D., and Constable, A. 2011. Autonomous video camera system for monitoring impacts to benthic habitats from demersal fishing gear, including longlines. Deep Sea Res. Pt. I Oceanogr. Res. Pap. **58**(4): 486–491. doi:10.1016/j.dsr.2011.02.006.

Krieger, K.J., and Wing, B.L. 2002. Megafauna associations with deepwater corals (*Primnoa* spp.) in the Gulf of Alaska. Hydrobiologia, **471**: 83–90. doi:10.1023/A:1016597119297.

Lagasse, C.R., Knudby, A., Curtis, J., Finney, J.L., and Cox, S.P. 2015. Spatial analyses reveal conservation benefits for cold-water corals and sponges from small changes in a trawl fishery footprint. Mar. Ecol. Prog. Ser. **528**: 161–172. doi:10.3354/meps11271.

Mortensen, P.B., and Buhl-Mortensen, L. 2004. Distribution of deep-water gorgonian corals in relation to benthic habitat features in the northeast channel (Atlantic Canada). Mar. Biol. **144**: 1223–1238. doi:10.1007/s00227-003-1280-8.

Pham, C.K., Diogo, H., Menezes, G., Porteiro, F., Braga-Henriques, A., Vandeperre, F., and Morato, T. 2014. Deep-water longline fishing has reduced

812

Can. J. Fish. Aquat. Sci. Vol. 75, 2018

impact on vulnerable marine ecosystems. Sci. Rep. **4**: 4837. doi:10.1038/srep04837. PMID:24776718.

R Core Team. 2015. R: a language and environment for statistical computing. R foundation for statistical computing, Vienna, Austria.

Reiswig, H. 2015. First Lanuginellinae (Porifera, Hexactinellida, Rossellidae) from the NE Pacific and first species of *Doconesthes* from the Pacific Ocean. Zootaxa, **3920**(4): 572–578. doi:10.11646/zootaxa.3920.4.6. PMID:25781403.

Rooper, C.N., Wilkins, M.E., Rose, C.S., and Coon, C. 2011. Modeling the impacts of bottom trawling and the subsequent recovery rates of sponges and corals in the Aleutian Islands, Alaska. Continental Shelf Res. **31**: 1827–1834. doi:10.1016/j.csr.2011.08.003.

Rooper, C.N., Zimmermann, M., Prescott, M.M., and Hermann, A.J. 2014. Predictive models of coral and sponge distribution, abundance and diversity in bottom trawl surveys of the Aleutian Islands, Alaska. Mar. Ecol. Prog. Ser. **503**: 157–176. doi:10.3354/meps10710.

Sainsbury, K.J., Campbell, R.A., Lindholm, R., and Whitelaw, A.W. 1997. Experimental management of an Australian multispecies fishery: examining the possibility of trawl-induced habitat modification. *In* Global trends: fisheries management. *Edited by* E.K. Pikitch, D.D. Huppert, and M.P. Sissenwine. American Fisheries Society. pp. 107–112.

Sampaio, I., Braga-Henriques, A., Pham, C., Ocaña, O., De Matos, V., Morato, T., and Porteiro, F.M. 2012. Cold-water corals landed by bottom longline fisheries in the Azores (north-eastern Atlantic). J. Mar. Biol. Assoc. U.K. **92**(7): 1547–1555. doi:10.1017/S0025315412000045.

Sinclair, A.F., Conway, K.W., and Crawford, W.R. 2005. Associations between bathymetric, geologic and oceanographic features and the distribution of the British Columbia bottom trawl fishery. *In* Annual Science Conference of the International Council for Exploration of the Sea, Scotland, UK, 20 September 2005. ICES CM 2005/L:25.

Stone, R.P. 2006. Coral habitat in the Aleutian Islands of Alaska: depth distribution, fine-scale species associations, and fisheries interactions. Coral Reefs, **25**: 229–238. doi:10.1007/s00338-006-0091-z.

Stone, R.P., Masuda, M.M., and Karinen, J.F. 2015. Assessing the ecological importance of red tree coral thickets in the eastern Gulf of Alaska. ICES J. Mar. Sci. **72**(3): 900–915. doi:10.1093/icesjms/fsu190.

Troffe, P.M., Levings, C.D., Piercey, G.E., and Keong, V. 2005. Fishing gear effects and ecology of the sea whip (*Halipteris willemoesi* (Cnidaria: Octocorallia: Pennatulacea)) in British Columbia, Canada: Preliminary observations. Aquat. Conserv. **15**: 523–533. doi:10.1002/aqc.685.

Wallace, S., Turris, B., Driscoll, J., Bodtker, K., Mose, B., and Munro, G. 2015. Canada's pacific groundfish trawl habitat agreement: a global first in an ecosystem approach to bottom trawl impacts. Mar. Pol. **60**: 240–248. doi:10.1016/j.marpol.2015.06.028.

Welsford, D., Sumner, M., and Ewing, G. 2014a. Estimates of the multi-gear footprint of the toothfish fishery at HIMI. *In* Demersal fishing interactions with marine benthos in the Australian EEZ of the Southern Ocean: an assessment of the vulnerability of benthic habitats to impact by demersal gears. *Edited by* D.C. Welsford, G.P. Ewing, A.J. Constable, T. Hibberd, and R. Kilpatrick. Australian Antarctic Division. pp. 199–210.

Welsford, D., Ewing, G., Constable, A., Hibberd, T., and Kilpatrick, R. 2014b. Demersal fishing interactions with marine benthos in the Australian EEZ of the Southern Ocean: an assessment of the vulnerability of benthic habitats to impact by demersal gears. Australian Antarctic Division. FRDC project 2006/042.

Williams, A., Schlacher, T.A., Rowden, A.A., Althaus, F., Clark, M.R., Bowden, D.A., Stewart, R., Bax, N.J., Consalvey, M., and Kloser, R.J. 2010. Seamount megabenthic assemblages fail to recover from trawling impacts. Mar. Ecol. **31**(S1): 183–199. doi:10.1111/j.1439-0485.2010.00385.x.

Woodby, D., Carlile, D., and Hulbert, L. 2009. Predictive modeling of coral distribution in the Central Aleutian Islands, USA. Mar. Ecol. Prog. Ser. **397**: 227–240. doi:10.3354/meps08358.

Wright, G., Ardron, J., Gjerde, K., Currie, D., and Rochette, J. 2015. Advancing marine biodiversity protection through regional fisheries management: a review of bottom fisheries closures in areas beyond national jurisdiction. Mar. Pol. **61**: 134–148. doi:10.1016/j.marpol.2015.06.030.

Wyeth, M.R., Kronlund, A.R., and Elfert, M. 2007. Summary of the 2004 British Columbia Sablefish (*Anoplopoma fimbria*) research and assessment survey. Can. Tech. Rep. Fish. Aquat. Sci. 2694. Fisheries and Oceans Canada, Nanaimo, B.C.